Surface Engineering

ISSN: 0267-0844 (Print) 1743-2944 (Online) Journal homepage: http://www.tandfonline.com/loi/ysue20

Oxygen effect on structural and optical properties of zinc oxide

Lamia Radjehi, Abdelkader Djelloul, Salim Lamri, Mohamed Fares Slim & Mourad Rahim

To cite this article: Lamia Radjehi, Abdelkader Djelloul, Salim Lamri, Mohamed Fares Slim & Mourad Rahim (2018): Oxygen effect on structural and optical properties of zinc oxide, Surface Engineering, DOI: 10.1080/02670844.2018.1515842

To link to this article: https://doi.org/10.1080/02670844.2018.1515842

Published online: 05 Sep 2018.

Submit your article to this journal

Article views: 2

View Crossmark data

Full Terms & Conditions of access and use can be found at
http://www.tandfonline.com/action/journalInformation?journalCode=ysue20

SURFACE ENGINEERING
https://doi.org/10.1080/02670844.2018.1515842

The Institute of Materials, Minerals and Mining

Taylor & Francis
Taylor & Francis Group

Check for updates

Oxygen effect on structural and optical properties of zinc oxide

Lamia Radjehi[a,b], Abdelkader Djelloul[a], Salim Lamri[b], Mohamed Fares Slim[b] and Mourad Rahim[c]

[a]Laboratoire des structures, propriétés et interactions inter atomiques (LASPI2A), Faculty of Science and Technology, Abbes Laghrour University, Khenchela, Algeria; [b]Laboratoire des Systèmes Mécaniques et d'Ingénierie Simultanée, Charles Delaunay Institute, University of Technology of Troyes, Nogent Antenna, High-Champagne Technology Center, Nogent, France; [c]Laboratoire d'Étude et de Recherche sur le Matériau Bois, IUT of Longwy, Cosnes-et-Romain, France

ABSTRACT

This article deals with an investigation of the effect of oxygen content on optical and structural properties of ZnO films. Zinc oxide films were deposited with the DC reactive magnetron sputtering process on Si(100) and glass substrates. ZnO films were elaborated at different oxygen flow rates from (O_2) 12 to 35 sccm. The evolution of optical and structural properties as a function of O_2 was investigated by X-ray diffraction, Profilometer, Field Emission Scanning Electron Microscopy (FESEM) and ultraviolet–visible. By increasing O_2, the crystallite size increases from 20 to 27 nm, which leads to an enlargement in the ZnO band gap from 3.18 to 3.30 eV. At 30 sccm of O_2, the films present a significant improvement in the band gap (3.30 eV). The results reveal that with increasing O_2, all films show a high crystallinity in the wurtzite phase and present a (002)ZnO preferential orientation along the *c*-axis. ZnO exhibited a good self-texture.

ARTICLE HISTORY
Received 22 May 2018
Revised 26 July 2018
Accepted 11 August 2018

KEYWORDS
ZnO; crystallite size; bad gap; self-texture; transmittance

Introduction

ZnO is a well-transparent conductive oxide, which has a wide energy band gap of 3.37 eV, good electrical conductivity of $10^3\ \Omega^{-1}\ cm^{-1}$, abundance, and environmentally friendly [1–3]. Because of its advantages, zinc oxide can be used in several applications like solar cells, optical and gas sensors, ultrasonic oscillators, transductors, transparent conductors and photoprotective coatings [4–8]. These applications depend on ZnO properties that are influenced by different factors like deposition conditions, chemical composition, ZnO structural, defects and preferential orientation. In zinc oxide thin films, the preferred orientation is a result of the surface free energy of the crystal plane, which results from a texture owing to the film itself (self-texture) or to epitaxy effects [9]. Thomas et al. have reported that ZnO films having crystallinity with predominant direction is a prerequisite for the fabrication of devices like UV diode lasers and acoustic–optic devices [7]. Many techniques including chemical vapor deposition (CVD) [10], spin coating [2], and chemical bath deposition [11], DC and RF magnetron sputtering [12] have been used to deposit the ZnO films. Among of them, DC magnetron sputtering is widely used in the semiconductor technology industries, because it has high deposition rate, low-cost, good adhesion with the substrate, low deposition temperatures required, and a good parameters control [1,8]. The deposition parameters such as working pressure, substrate temperature, type of substrates, and O_2 flow rate influence the different thin film properties [9]. Many researchers have discussed the correlation between properties of doped zinc oxide and oxygen concentration. Thomas et al. have studied the O_2 flow effect rate in textured grain growth, the band gap and the resistance of ZnO films are elaborated by the SILAR method. Cao et al. have fabricated ZnO:Al (AZO) thin films on quartz substrates using the pulsed laser deposition (PLD) method at different O_2 flow rates. They found that increasing O_2 leads to an increase of both the Al content and the grain size, which influence the AZO transmittance (90%) and the E_g (3.48 eV) [13]. Jung et al. reported that the refractive index and extinction coefficients of ZnO:I (IZO) films have been changed with DC magnetron sputtering parameters such as O_2 flow rate, deposition temperature, and sputtering gas. It was found that at 250°C and without additional oxygen gas, the IZO films showed a best electrical of 361 μΩ cm, presenting a smooth morphology and high optical transmittance [14]. These researchers indicate that the concentration of oxygen has a significant impact on the properties of doped ZnO films elaborated by a different process. However, a few studies of the O_2 effect on zinc oxide film properties were reported, which is not so clear, so further investigations are much needed. In this paper, we have deposited the ZnO films using DC reactive magnetron sputtering at different O_2 flow rates. Evolution structure and microstructure with increasing O_2 were reported. The

CONTACT Lamia Radjehi lamia.radjehi@gmail.com Laboratoire des structures, propriétés et interactions inter atomiques (LASPI2A), Faculty of Science and Technology, Abbes Laghrour University, Khenchela 40000, Algeria

© 2018 Institute of Materials, Minerals and Mining Published by Taylor & Francis on behalf of the Institute

relationship between the band gap enlargement and the oxygen vacancy decreased which is due to an increase of O_2. The correlation between optical and structural properties was investigated. The films were elaborated on an amorphous glass substrate that permits us to study the self-texture of ZnO thin films with the pole figure.

Experimental details

The ZnO thin films were deposited by a DC magnetron sputtering unit (Alcatel SCM600). The Zn target (99.9% purity, 200 mm diameter) was fixed on a magnetron-effect cathode. The substrate holder was placed in front of the target at 140 mm distance. Oxygen was used as reactive gas mixtures with argon. Argon was fixed at 40 sccm, whereas O_2 was varied between 12 and 35 sccm. Before the film deposition, the chamber pressure was pumped down to 10^5 mbar. The square glass substrates (2.5×2.5 cm^2) and Si(100) wafers (1×1cm^2) were cleaned in acetone and ethanol (5 min for each one) before their introduction in the deposition chamber. In order to remove the contaminated surface, the Zn target was pre-sputtered in a pure argon atmosphere at 450 V and 0.4 Pa. The working pressure was performed at 0.5 and an electrical intensity of 1 A. The deposition parameters are listed in Table 1. The film thickness was measured using a profilometer (AltiSurf). The ZnO crystalline structure was analysed by X-ray diffraction (XRD) using a D8 advanced, with a $Cu_{K\alpha}$ radiation source (40 kV, 40 mA, λ_{Cu}=0.154 nm). The crystallite size (D) was estimated from the width half-maximum of the (002)ZnO orientation using Scherrer's formula [15]:

$$D = \frac{0.94\lambda}{\beta_{(002)} \cos \theta_{(002)}} \quad (1)$$

where 0.94 is a shape factor, λ represents the X-ray wavelength of the radiation source used for the measurement (λ_{Cu}=0.154 nm), β(rad) is the line width full width half maximum, and θ is the Bragg's angle.

The lattice parameter (c) for the (002)ZnO orientation can be determined by the equation

$$d_{hkl} = \frac{1}{\sqrt{\frac{4(h^2+k^2+hk)}{3a^2} + \frac{l^2}{c^2}}} \quad (2)$$

Table 1. Deposition parameters of the ZnO films.

Deposition parameters	Value
Electrical intensity	1 A
Substrate temperature	68 °C
Work pressure	0.5 Pa
Base pressure	1×10^{-5} mbar
Deposition time	40 min
Oxygen flow ratio	12,15, 20, 25, 28, 30 and 35 sccm
Argon flow ratio	50 sccm

where the inter-reticular distance is

$$d_{hkl} = \frac{\lambda}{2 \sin \theta_{hkl}} \quad (3)$$

The microstrains of the (002)ZnO orientation were calculated using Equation (4):

$$\varepsilon = \frac{\Delta c}{c_{bulk}} \quad (4)$$

where ε is the microstrain in the direction of the c-axis, i.e. perpendicular to the substrate surface $\Delta c = c_{film} - c_{bulk}$, c_{film}, and c_{bulk} of the ZnO hexagonal phase.

The cross-sectional and the film morphology were observed by using a field emission scanning electron microscope (FE-SEM-Hitachi-SU8030) which was equipped with a microanalyse X spectrometer to determine the chemical composition of the films. The transmittance of films synthesised on the glass substrates was measured by using a Perkin Elmer UV–VIS Lambda 19 spectrophotometer in the 190–800 nm spectral range.

Results and discussion

Crystalline structure

Figure 1 presents XDR spectra of ZnO films at various O_2 flow rates (from 12 to 35 sccm). At 12 and 15 sccm, weak peaks (002) and (101) appeared at 36.49°and 43.47° which were attributed to the Zn pure phase (JCPDS card No#1-1238). In addition, other peaks were seen at 31.77°(100), 34.42° (002),62.86° (103), and 72.56° (004), which may be assigned to the presence of the ZnO phase (JCPDS Card No#36-1451). From 20 to 35 sccm of oxygen, the Zn phase completely disappeared; however, the (002)ZnO peak becomes predominant in parallel with a weak (100),(103), and (004) peaks located at 31.77°, 62,86°, and 72,56° which can be attributed to the ZnO wurtzite phase.

From 20 sccm, the peaks become sharper with higher intensity [8]. In addition, the (002)ZnO peak intensity is considerably enlarged with increasing O_2. Therefore, the increasing O_2 enhances the formation of the ZnO phase. Furthermore, the (002)ZnO peak position was shifted towards the higher diffraction angles with increasing O_2, which is attributed to the change on a film composition (Figure 1). It can be explained with oxygen insertion in the Zn crystal lattice to form the ZnO phase. It leads to a change in the lattice constants and induces compressive strain by reducing the voltage target ion bombardment energy (Table 2) [16].

Figure 2 shows the evolution of the deposition rate and the average crystallite size as a function of O_2. In magnetron sputtering, the oxygen served mainly as a reaction source, but Ar served as the sputter Zn target.

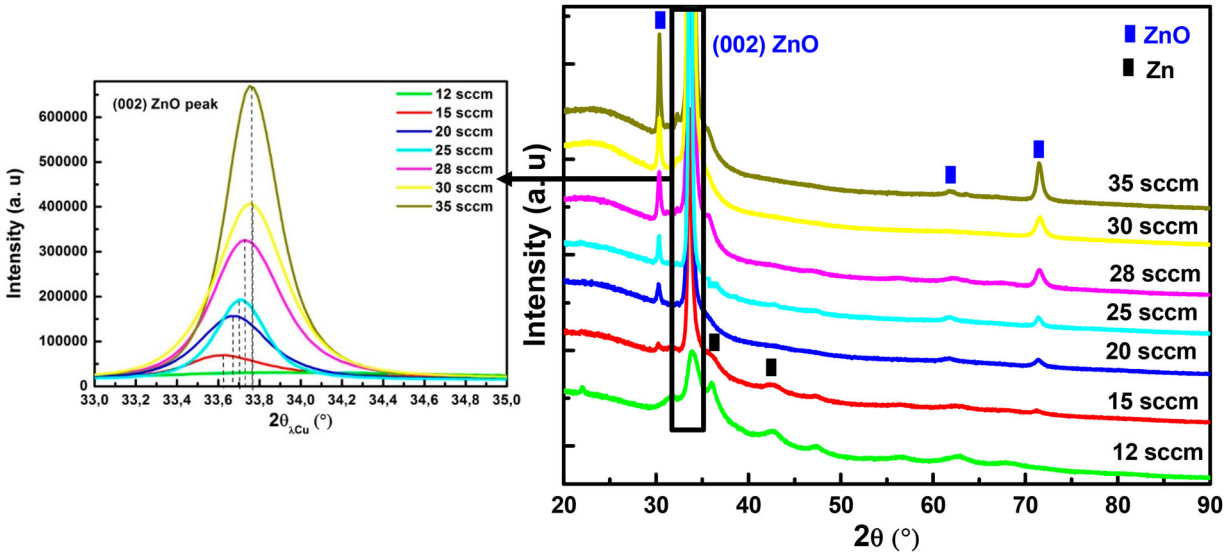

Figure 1. The XRD spectra of ZnO films at different O_2 flow rates.

Table 2. Lattice parameter (*c*), lattice microstrains and film thickness of ZnO films.

ZnO	Lattice parameter (*c*), nm	Lattice strain (%)	Peak positions (°)	Film thickness (nm)
12 sccm	0.52053	−0.02516	33.57	1718
15 sccm	0.52514	0.86025	33.62	800
20 sccm	0.52578	0.60698	33.67	653
25 sccm	0.52413	0.66627	33.70	300
28 sccm	0.52479	0.79303	33.72	250
30 sccm	0.52367	0.57792	33.77	220
35 sccm	0.52408	0.65667	33.77	200

The abundant presence of Ar gas in the sputtering chamber leads to high sputtering yield with a speed rate, which is related to the molecule number of Ar per unit volume. At 12 sccm, the ZnO film shows a high film thickness and deposition rate of 1790 nm and 44.75 nm/min, respectively (Table 2). By increasing O_2, the thickness of the films and the deposition rate decreased until 5 nm/min and 200 nm (at 35 sccm), respectively, which is a result of the target position with oxygen [3]. It was seen that the increase of O_2 leads to the increase of the crystallite size

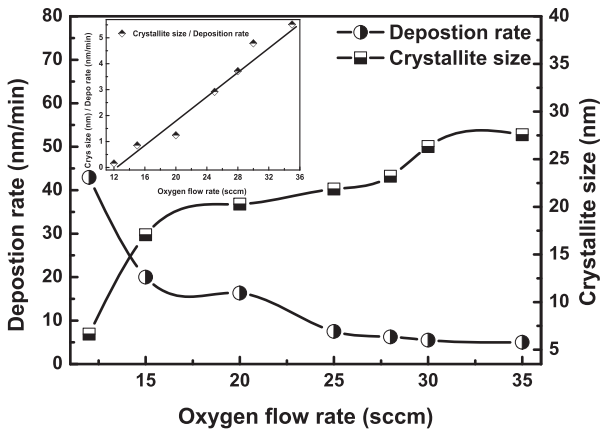

Figure 2. Deposition rate and crystallite size of the deposited ZnO films as a function of O_2.

(Figure 2). At 12 sccm, the film corresponding to a mixture of Zn and ZnO (Figure 1) presents a lower crystallite size value of 6 nm. However, from 15 sccm of O_2, ZnO films have an average value between 17 and 27 nm. It was seen that the decrease up to 112 nm of the crystallite size of ZnO films was elaborated by spin coating for higher thickness [2]. We can see that the ratio between the deposition rate and the crystallite size as a function of O_2 is linear (Figure 2).

Morphology and chemical composition

The stoichiometry of the ZnO films was determined by using microanalysis X as presented in Table 3. The O/Zn ratio was increased until about 1 and the film stoichiometry was changed with increasing O_2. At a lower oxygen flow rate, the ZnO is under stoichiometric because of the presence of the defect that was produced during the deposition process. Thus, the presence of the oxygen vacancy is owing to the decrease in the oxygen content.

Figure 3 presents the FESEM fractured cross-sectional and the surface morphology images of the ZnO films with different O_2. At 12 sscm, the zinc oxide films show a cauliflower-like form with the appearance of micro-droplets and craters in the free surface morphology [18]. According to Andres's SZM [19], the film structure corresponds to the zone T structure caused by the compressive strain state film (ε=

Table 3. Atomic percentage of ZnO films at different O_2 flow rates.

Oxygen flow rate (sccm)	O at.-%	Zn at.-%	O/Zn
12	43.26	56.74	0.76
15	45.55	54.45	0.84
20	46.13	53.87	0.86
25	48.87	51.13	0.95
28	49.07	50.93	0.96
30	49.47	50.53	0.98
35	50.79	49.21	1.03

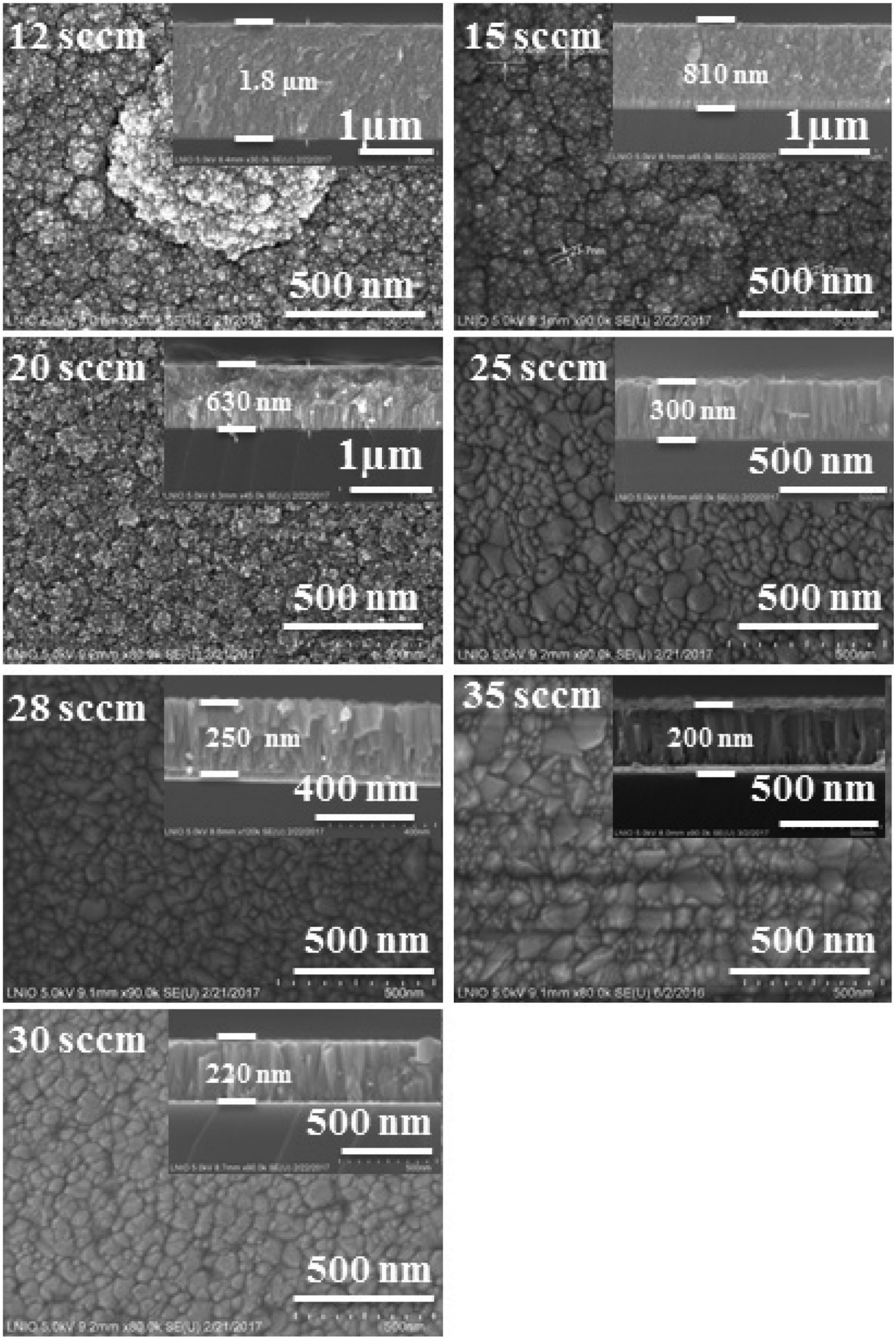

Figure 3. The FESEM cross-sectional and surface morphology of the ZnO films as a function of O_2.

−0.02516). It is owing to the mutual interference of the intermediate Zn and ZnO phases (Figure 1). With an increase in O_2, the heterogeneous grain size varied between 21 and 114 nm with the spherical shape distributed throughout the surface [3]. According to Andres's SZM, the film structure corresponds to the zone 2 [19,20].

Texture

The {002}, {101} and {103} experimental pole figures of the ZnO film (30 sccm) are shown in Figure 4. The direct pole figures are presented in a stereographic projection for declination angles (ψ) up to 70°. The as-deposited film presents a {002} fibre texture along the *c*-axis which is perpendicular to the substrate surface. However, the crystallographic direction of the ZnO film does not exhibit a perfect symmetry revolution around the fibre axis. At the {101} pole figure, we can observe an incomplete ring around ϕ=60° and ψ=65°, which is coherent with the theoretical value (the ring should appear at ψ=61.6°), that is more intense at −40°<ϕ<50 and 130°< ψ <210°. At the {103} direct pole figure, we can observe a first ring with a low intensity around ψ=31° and a high intense ring between ψ=65° and ψ=70°. This can be explained by the favoring of some directions instead of others. This may be due to the angle formed between the normal surface of the substrate and the coating vapour flux [21]. This result is in agreement with that performed by Fujimura et al., which explains that zinc oxide has the wurtzite structure and the direction of each apex is parallel to the *c*-axis. In the ZnO structure, the (002) plane is the closely packed, which has the lowest surface free energy. This is why the ZnO film tends to grow towards the [002] direction and it has the self-texture towards (002) [22].

Optical properties

Figure 5 shows the transmittance in the UV–VIS regions of the deposited ZnO films at 15, 20, 25, 28, 30 and 35 sccm. All samples present a large absorption in the UV region and a good transparency in the visible wavelength range. The absorption edge is around 375 nm for all the films. The increase of O_2 leads to improvements in the film transmittance until 80% at the 500 nm visible region. The inter-band absorption is well marked and close to that of the ZnO even if there is an optimisation to reach the 3.37 eV. With the fringe number films elaborated at 25, 28, 30 and 35 sccm, the layers show small size dispersion. Therefore, at 12–20 sccm, the layers created more free carriers, hence the low transmission. To estimate the optical absorption coefficient (α), we have used the relationship of transmittance as [23]

$$\alpha = \frac{1}{d}\ln(T) \tag{5}$$

with d being the film thickness. In addition, the UV transmittance (T) is directly linked to the optical band gap. The relationship between E_g and the T can be obtained as [24]

$$\alpha h\nu = A(h\nu - E_g)^n \tag{6}$$

where α is the absorption coefficient, A is a constant, $h\nu$ is the photon energy, h is the Plank constant, E_g is the optical band gap, and n = 1/2 for direct semiconductors.

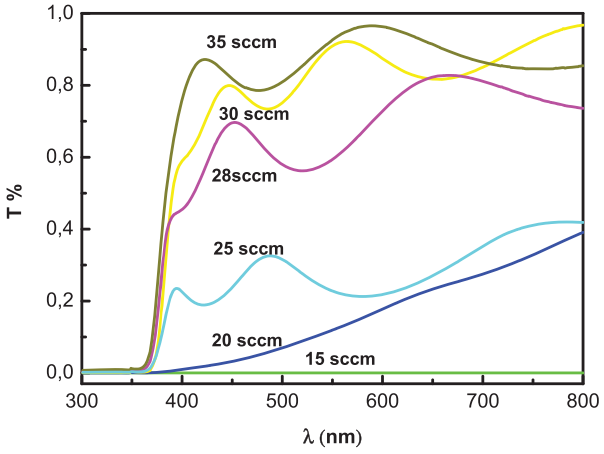

Figure 5. Transmission as a function of O_2 of the ZnO/glass sample.

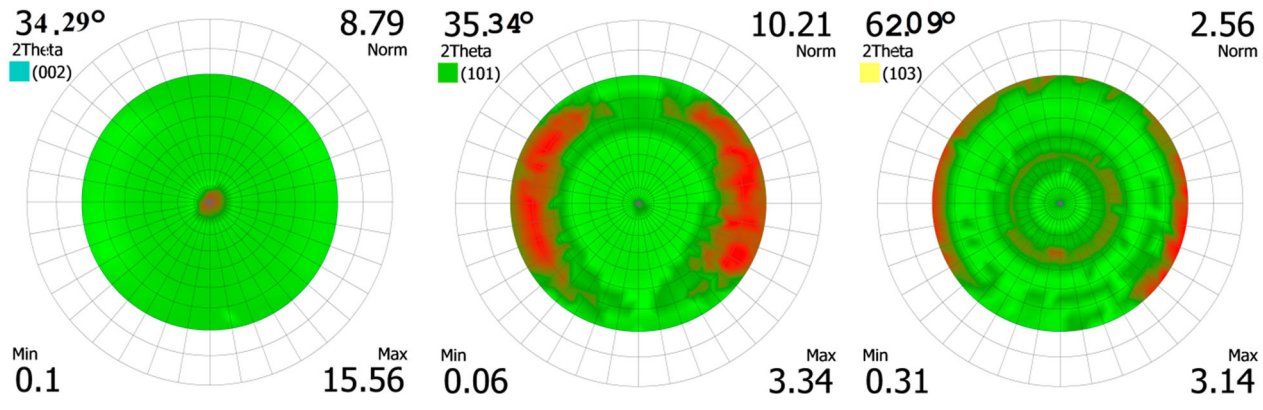

Figure 4. Direct pole figures {002}, {101} and {103} determined by Diffract-texture software of ZnO/glass sample.

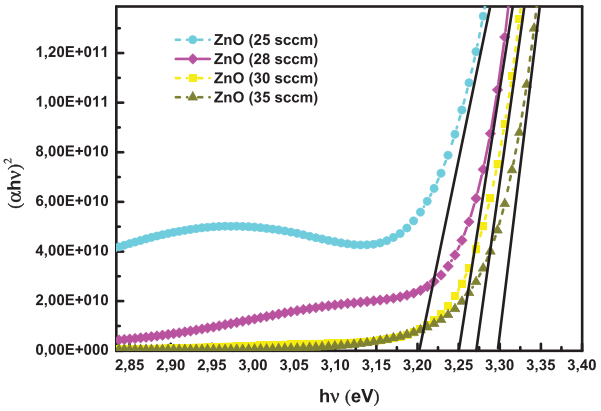

Figure 6. Optical band gap energy as a function of O_2 of the ZnO/glass sample.

Figure 6 shows the evolution of $(\alpha h\nu)^2$ versus $h\nu$ of zinc oxide film at 25, 28, 30, and 35 sccm of O_2. E_g was calculated from the extrapolation of the linear part of $(\alpha h\nu)^2$ versus $h\nu$ data (at $\alpha = 0$). At 25, 28, 30 and 35 sccm, the films have an optical energy gap of 3.18, 3.23, 3.26 and 3.30 eV, respectively. The shift of the absorption edge to shorter wavelengths indicates that E_g increases with increasing O_2. Zhu et al. found that the increases in the O_2:Ar ratio suggested a wavelength red shift compared to E_g of intrinsic ZnO (3.37 eV) because of stress film state [17]. Dutta [25] and Bedia et al., [26] reported that the grain size increase attributed to the band bending reduction in the grain boundaries, which leads to increase of E_g. Therefore, Zhang et al. [27] have explained that the substrate temperature increase is the reason for increase in the grain sizes, which leads to the enlargement of the E_g in ZnO films. In our study, the shift absorption edge of the band gap from 3.18 (25 sccm) to 3.30 eV (35 sccm) may be attributed to the grain size increase.

On the other hand, the band gap increase is related to the lower carrier density introduced by oxygen vacancies in the ZnO film, which is owing to the increasing oxygen flow. Moreover, when oxygen vacancy appears in the ZnO structure, the oxygen vacancy states become nonlocalised and the valence band rose. Therefore, a decrease in the oxygen vacancy concentration leads to a decrease in the extended nonlocalisation, resulting in increasing of the band gap [28].

Conclusion

This paper focuses on the effect of the oxygen flow rate (O_2) on the structure, the morphology and the optical properties of ZnO films. The deposited process is carried out according to the DC magnetron sputtering technique. Between 12 and 15 sccm, the deposited films showed a cauliflower-like columnar structure with a mixture of Zn and ZnO. However, the films present a (002)ZnO preferential orientation and the structure becomes spherical in shape from 20 sccm.

The ZnO crystallite size increased but the lattice parameter decreased as the O_2 increased. The film deposited at 30 sccm of oxygen shows best optical and structural properties. It presents a {002} fibre texture with the *c*-axis perpendicular to the substrate surface.

In addition, its optical transmittance (at 500 nm) and its band gap of ZnO films increased to reach high values of 88.7% and 3.3 eV, respectively. Band gap enlargement was owing to decrease in the oxygen vacancy, which is a result of increasing O_2.

Disclosure statement

No potential conflict of interest was reported by the authors.

References

[1] Wang Y, Peng ZJ, Wang Q, et al. Tunable electrical resistivity of oxygen-deficient zinc oxide thin films. Surf Eng. 2017;33:217–225. doi:10.1080/02670844.2016.1212519
[2] Rahman A, Jayaganthan R. Study of nanostructured Co and Al Co-doped ZnO films fabricated by electroless technique. Surf Eng. 2016;31:372–377. doi:10.1179/1743294415Y.0000000079
[3] Ravichandran K, Sindhuja E, Uma R, et al. Photocatalytic efficacy of ZnO films – light intensity and thickness effects. Surf Eng. 2017;33:512–520. doi:10.1080/02670844.2016.1270797
[4] Amuthasurabi M, Chandradass J, Seong-Ju P, et al. Reduction of self-heating effect in (Ga)ZnO thin film transistor. Surf Eng. 2018;34:816–819.
[5] Manivasaham A, Ravichandran K, Subha K. Light intensity effects on the sensitivity of ZnO:Cr gas sensor. Surf Eng. 2017;33:866–876. doi:10.1080/02670844.2017.1331724
[6] Yu J, Gao Y, Wang L, et al. Anti-reductive properties of AZO/FTO bilayered transparent conducting films. Surf Eng. 2018;185:222–227.
[7] Thomas D, Vattappalam SC, Mathew S, et al. Studies on effect of oxygen flow rate in textured grain growth of ZnO thin films. Mater Sci Eng. 2015;73:1–5.
[8] Thomas D, Vattappalam SC, Mathew S, et al. Studies on effect of oxygen flow rate in textured grain growth of ZnO thin films. Mater Sci Eng. 2015;73:1–5.
[9] Kasuga M, Mochizuki M. Orientation relationships of zinc oxide on sapphire in heteroepitaxial chemical vapor deposition. J Cryst Growth. 1981;54:185–194. doi:10.1016/0022-0248(81)90459-0
[10] Sameem MS. Effect of substrates and film thickness on the properties of ZnO thin films grown by chemical bath deposition. Int J Res Sci Eng Technol. 2015;II:19.
[11] Amuthasurabi M, Chandradass J, Seong-Ju P, et al. Reduction of self-heating effect in (Ga)ZnO thin film transistor. Surf Eng. 2017;33:816–819. doi:10.1080/02670844.2017.1294813
[12] Vinoth E, Gowrishankar S, Gopalakrishnan N. RF magnetron sputtered Cd doped ZnO thin films for gas-sensing applications. Mater Manuf Process. 2017;32:377–382. doi:10.1080/10426914.2016.1244834
[13] Cao PJ, Han S, Liu WJ, et al. Effect of oxygen flow rate on optical and electrical properties in Al doped ZnO thin films. Mater Technol Adv Perfor Mater. 2014;29 (6):1753–5557.
[14] Jung YS, Seoa JY, Lee DW, et al. . Influence of DC magnetron sputtering parameters on the properties

of amorphous indium zinc oxide thin film. Thin Solid Films. 2003;445(6):63–71.
[15] Aissani L, Nouveau C, Walock MJ, et al. Influence of vanadium on structure, mechanical and tribological properties of CrN coatings. Surf Eng. 2015;31:779–788. doi:10.1179/1743294415Y.0000000043
[16] Aissani L, Fellah M, Nouveau C, et al. Structural and mechanical properties of Cr–Zr–N coatings with different Zr content. Surf Eng. 2017;33:1743–2944.
[17] Zhu Hua, Wang Hemei, Wan Wenqiong. Influence of oxygen and argon flow on properties of aluminum-doped zinc oxide thin films prepared by magnetron sputtering. Thin Solid Films. 2014;566:32–37. http://dx.doi.org/10.1016/j.tsf.2014.07.021
[18] Zhu H, Wang H, Wan W, et al. Influence of oxygen and argon flow on properties of aluminum-doped zinc oxide thin films prepared by magnetron sputtering. Thin Solid Film. 2014;566:32–37. doi:10.1016/j.tsf.2014.07.021
[19] Silva PS, Edinéia P, Schmitz S, et al. Electrodeposition of Zn and Zn–Mn alloy coatings from an electrolytic bath prepared by recovery of exhausted zinc–carbon batteries. J Power Sources. 2012;210:161–121. doi:10.1016/j.jpowsour.2012.03.021
[20] He HY, Shen Q. Template effects of microstructure and property of sol–gel-deposited ZnO:Al:Mo films. Mater Manuf Process. 2014;29:1157–1161. doi:10.1080/10426914.2013.840914
[21] Sohn YH, Biederman RR, Sisson RD Jr, et al. Microstructural development in physical vapour-deposited partially stabilized zirconia thermal barrier coatings. Thin Solid Films. 1994;250:1–7. doi:10.1016/0022-0248(93)90861-P
[22] Fujimura N, Nishihara T, Goto S, et al. Control of preferred orientation for ZnOx films: control of self-texture. J Crystal Growth. 1992;130:269–279. doi:10.1016/0022-0248(93)90861-P
[23] Tauc J. Amorphous and liquid semiconductor. London: Plenum Press; 1974.
[24] Samiyammal P, Parasuraman K, Prabha D, et al. Optical and magnetic properties of Ba-doped CdS thin films. Surf Eng. 2017;33:835–840. doi:10.1080/02670844.2017.1303981
[25] Dutta V. Spray deposited ZnO nanostructured layers for dye sensitized solar cells. Energy Procedia. 2011;3:58–62. doi.org/10.1016/j.egypro.2011.01.010
[26] Bediaa A, Bediaa FZ FZ, Aillerieb M M, et al. Morphological and Optical properties of ZnO thin films prepared by spray pyrolysis on glass substrates at various temperatures for integration in solar cell. Eng Procedia. 2015;74:529–538. doi:10.1016/j.egypro.2015.07.740
[27] Zhang X, Ma S, Liu F, et al. Effects of substrate temperature on the growth orientation and optical properties of ZnO:Fe films synthesized via magnetron sputtering. J Alloys Compd. 2013;574:149–154.
[28] Liu H, Zeng F, Lin Y, et al. Correlation of the oxygen vacancy variations to the band gap changes in epitaxial. Appl Phys Lett. 2013;102:181908. doi:10.1063/1.4804613